Tracking Vehicles Equipped with Dedicated Short-Range Communication at Traffic Intersections

Patrick Emami
University of Florida
Gainesville, FL, USA
pemami@ufl.edu

Lily Elefteriadou
University of Florida
Gainesville, FL, USA
elefter@ce.ufl.edu

Sanjay Ranka
University of Florida
Gainesville, FL, USA
sanjayranka@gmail.com

ABSTRACT

In the near future, the traffic stream will contain both connected and autonomous vehicles with Dedicated Short-Range Communication (DSRC) vehicle-to-infrastructure (V2I) capabilities. With these new technologies, it will become possible to optimize the performance of traffic intersections so that wasted time at red lights and carbon emissions are minimized. Sensors, such as Doppler radar and traffic cameras, can use the data received at Road-Side Units (RSUs) from DSRC-equipped vehicles to assist with tracking and classifying all of the traffic approaching an intersection. In order to fuse information between multiple sensors, each sensor at the traffic intersection needs to compute the uncertainty about its estimate of the state of every vehicle it is tracking. In this work, we evaluate different tracking filters for their ability to estimate the state of a vehicle approaching a traffic intersection based on GPS data received over DSRC. We ran experiments with a vehicle equipped with a Cohda Wireless Mk5 On-Board Unit (OBU) and a high-precision GPS sensor to generate ground-truth data. We present a comparison of the performance of a linear Kalman filter, extended Kalman filter, and particle filter configured with different kinematics models. The effects of measurement bias in the GPS data in DSRC messages is also explored; we observe that without any bias estimation, the performance of the track filters degrades significantly.

KEYWORDS

Tracking; V2I; DSRC; Kalman filter; particle filter

1 INTRODUCTION

The rapid adoption of automated and connected vehicle technologies, such as the installation of V2I communications devices in vehicles and at traffic intersections, will allow for the deployment of many intelligent transportation systems (ITS) projects that will enhance the efficiency and safety of transportation [9]. One such application is intelligent intersection control, where a controller jointly optimizes signal timings and the trajectories of automated vehicles so that the overall throughput of the intersection is maximized. There have been several proposed systems for optimizing isolated intersection performance that rely on having complete information about the traffic approaching the intersection [18] [23] [14]. One way to accomplish this is to equip vehicles with DSRC, which enables them to broadcast their position and speed to other vehicles and nearby infrastructure. The Society of Automotive Engineers has published a safety standard for connected vehicle communication that requires 68% of GPS points sent in Basic Safety Messages (BSMs) to fall within a circle of radius 1.5 meters around the vehicle's true position [6]. To obtain the desired tracking precision for traffic intersection optimization or other related ITS applications, an estimate of the uncertainty in the GPS extracted from a BSM is needed. However, environmental effects, such as multipath, can add hidden biases to the GPS measurements that are difficult to estimate and filter out. This is especially prevalent in urban canyons, which are stretches of narrow road in urban areas with tall buildings and trees lining the road. Signal reflections from tall buildings, trees, and other vehicles may cause interference at GPS receivers which introduces biases in the GPS measurements.

In this work, we evaluate different tracking filters for estimating the state of vehicles approaching two urban traffic intersections in Gainesville, FL, based on GPS data received over DSRC. The most common approach used in the literature for tracking an object given the presence of nonlinearities in the equations that govern the system is the extended Kalman filter (EKF). The EKF is a suboptimal filter designed to account for nonlinearities in the state and measurement processes. The classic linear Kalman filter (LKF) makes the strong assumption that the state and measurement processes are described by linear functions. Under the additional assumption that the noise in the state and measurement processes can be modeled by a mean-zero Gaussian distribution, both filters perform favorably and are reasonably easy to implement. When there is significant nonlinearity present or the noise is generated by a non-Gaussian distribution, the particle filter (PF) can be used instead for state estimation.

The main contributions of this paper are:

- We evaluate the precision and accuracy of GPS data from a Cohda Wireless Mk5 DSRC unit
- We compare the ability of constant velocity and constant acceleration kinematics paired with the LKF, EKF, and PF to model the trajectories of vehicles approaching traffic intersections
- We analyze the robustness of each filter in the presence of GPS measurement biases

Our experimental results suggest that without GPS bias estimation, the tracking filters actually produce worse state estimates than simply using the unfiltered GPS. Indeed, modeling the GPS's noise distribution incorrectly with a mean-zero Gaussian distribution resulted in poor tracking performance for all filters. Mitigating

DIVANet'17, November 21–25, 2017, Miami, FL, USA

ACM ISBN 978-1-4503-5164-5/17/11…$15.00
https://doi.org/10.1145/3132340.3132356

the effects of measurement bias remains an area of active research. Since no information about the raw GPS signal is contained in the BSM, methods that leverage contextual information about the environment to address multipath appear to be promising [21].

The remainder of the paper is organized as follows. In Section 2, we discuss related works in tracking and sensor fusion for ITS applications. In Section 3, we present an empirical analysis of the accuracy and precision of our OBU and describe our formulation of the LKF, EKF and PF for tracking vehicles at traffic intersections. In Section 4, we evaluate the performance of the three filters with real data generated by an instrumented vehicle. In Section 5, we discuss future work and conclude the paper.

2 RELATED WORKS

Traffic surveillance at urban intersections is a relatively open problem with many challenges and has only recently received significant attention as cheap and powerful sensors have become available. As the penetration rate of vehicles equipped with V2I sensors increases, more data becomes available to be fused with traditional sensing modalities such as cameras and radar. The benefits of leveraging data fusion for ITS applications are plentiful; [9] demonstrated via simulations that vehicle-to-X (V2X) technology will significantly reduce travel times in smart cities, and [10] discusses many other areas where data fusion can have an impact in ITS.

In [4], the authors described a methodology for tracking vehicles from a host vehicle based on DSRC and radar fusion. They used Kalman filters to track surrounding vehicles, which provided them with an estimate of the uncertainty in the GPS data they received via DSRC. They emphasized that the GPS from DSRC alone is, in general, not accurate enough for safety applications; this motivated their decision to fuse the GPS data with radar. However, they did not consider the effects of biases from external sources, such as multipath, when designing their Kalman filter. Another work involving multisensor fusion with GPS data from V2X is [17], which proposed a data fusion system that fused localization information obtained from vehicle-to-vehicle (V2V) communication with video data. Interestingly, in [16] and [19], the authors demonstrated that multiple vehicles equipped with low-cost GPS sensors are able to share position information via V2V technology to improve their own individual state estimates. [16] also assumed that the effect of measurement bias was negligible and simply used a mean-zero Gaussian distribution with a small (0.5 m) standard deviation for the GPS measurement uncertainty in their Kalman filter.

A relevant experimental study by [12] showed that V2X communications are significantly affected when line-of-sight with the receiver is obstructed. This has serious implications from a tracking perspective, since a large vehicle blocking a connected vehicle's line-of-sight with the traffic intersection could prevent it from transmitting BSMs, as well as occlude it from view of video cameras and other sensors. A methodology for vehicles to obtain precise localization information based on other data in GPS-denied environments is presented in [13], which could prove essential for applications such as tracking at urban traffic intersections.

Figure 1: Most of the data is collected from driving in the southbound lane at SW 42nd and SW 40th St in Gainesville, FL, highlighted in this image. This stretch of road is lined with many trees and buildings, and experiences medium-level traffic. All of these can potentially reflect GPS signals that interfere with the GPS receiver on a DSRC-equipped vehicle.

3 VEHICLE STATE ESTIMATION

We extend the aforementioned researches by evaluating three well-known tracking filters for the purpose of tracking individual DSRC-equipped vehicles. The next section presents the methodology for addressing our tracking problem, beginning with an empirical analysis of the uncertainty in the GPS data sent in BSMs from our DSRC unit.

3.1 DSRC GPS Analysis

We consider a scenario where one or more vehicles approaching an intersection are instrumented with DSRC via an OBU. There is a Road-Side-Unit (RSU) present at the intersection set up to receive BSMs transmitted from the OBUs on the 5.9 GHz band dedicated for ITS applications [7]. The OBUs are designed to transmit a BSM at a fixed interval, e.g., at 10 or 20 Hz. The standard message structure for a BSM is described in [5]. The accuracy and precision of the localization information contained in the BSM is dependent on the quality of the GPS signal available to the OBU and the performance of any internal filtering implemented by the manufacturer of the OBU. The Wide Area Augmentation System (WAAS) provides GPS corrections to our OBU, which reduces the uncertainty in the position estimates to at most 2-3 meters in latitude and longitude; WAAS is the recommended system for providing GPS corrections for connected vehicle applications [6].

We carry out tracking in the Universal Transverse Mercator (UTM) system; this allows us to convert GPS coordinates to a system that is locally Cartesian, uses interpretable units, and is amenable to simple trigonometric calculations [15]. UTM Northing is aligned with true north and refers to the north-south direction, and UTM Easting refers to the east-west direction.

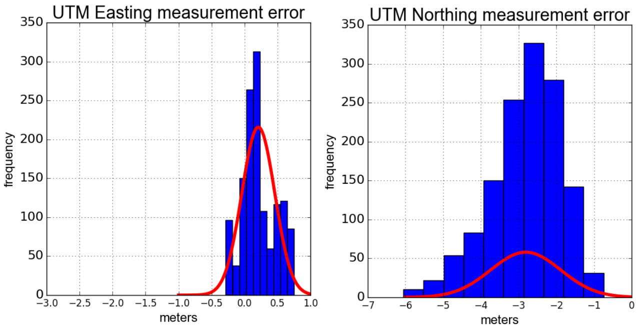

Figure 2: Histograms of the error between the time-aligned GPS data points in UTM Easting and Northing. Fitting a Gaussian distribution to the UTM Northing error histogram results in a mean of -2.81 meters and standard deviation of 0.93 meters. For UTM Easting, the mean is 0.21 and standard deviation is 0.25.

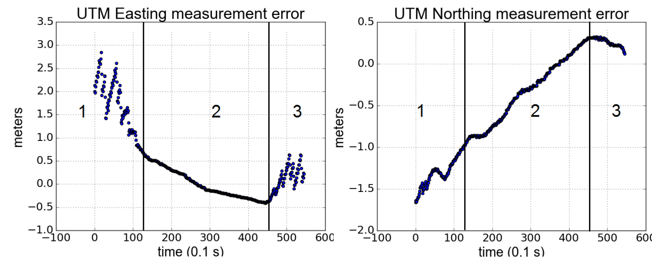

(a) **(b)**

Figure 3: Error in UTM Easting (a) and Northing (b) over the duration of an intersection approach where the vehicle stopped at a red light. In the first segment (1) between 0 and 120 (units of 0.1 seconds), the vehicle is decelerating to a stop. The next segment (2) between 120 and 450 shows the measurement error when the vehicle is stopped at the light. Following this, the final segment (3) shows when the vehicle accelerates and drives through the intersection.

The noisy measurement of a vehicle's state at discrete time step k can be obtained from a BSM as

$$o_k = [x_k, y_k, \theta_k, v_k]^\top \tag{1}$$

In Equation 1, x_k is UTM Easting, y_k is UTM Northing, θ_k is the heading of the vehicle in degrees clockwise from true north, and v_k is the speed of the vehicle in meters/s.

A similar analysis of the GPS from a stationary OBU suggests that the noise distribution has very low variance but a time-varying bias, and can be approximated by a Gaussian distribution with zero mean and standard deviation of 1.125 meters in latitude and longitude [11]. Similarly to [11], we compare the GPS from the DSRC OBU directly with a Novatel V3-HP GPS sensor with Omnistar subscription service. This high-precision sensor provides absolute localization with an error of between 0.1 and 0.5 meters when the service is available [8]. When unable to access the service, the sensor defaults to a differential GPS solution, CDGPS, which provides sub-meter precision. The output of this GPS sensor is in turn fused with inertial and odometry information to obtain extremely precise positioning.

The GPS antennas for the Novatel and DSRC are attached to the roof of the vehicle on the back axle close to the center of the vehicle. To generate the data, the vehicle is driven towards an intersection (see Figure 1) starting from a location about 600 feet away. The vehicle's heading is 180 degrees from true north and it reaches speeds between 20 and 40 mph. The BSMs sent by the DSRC OBU and the readings from the high-precision GPS sensor are timestamped and recorded; a total of over 3000 data points are collected over multiple runs. We align the data by the timestamps corresponding to when the BSM and high-precision GPS measurements were generated; each timestamp consists of UTC time from the GPS satellites sending the data. In the SAE safety standard, the requirement for the accuracy of the timestamp is in each BSM is within 1 ms of a reference UTC source [6]. However, time synchronization errors when aligning data for tracking is still a possibility when different DSRC hardware and software is used by the vehicles and intersection, as well as when accounting for the transmission time of a BSM. The errors in UTM Easting and Northing are depicted in Figure 2.

As can be seen in Figure 2, the errors in UTM Northing are greater than in UTM Easting. One possible source of the measurement bias observed here is a slight time synchronization error between the two GPS units. Furthermore, the GPS receiver in the Cohda Wireless Mk5 is susceptible to multipath and other sources of GPS error common in urban environments that may become more pronounced depending on the current GPS satellite geometry and the speed of the vehicle [22]. We observed that as the speed of the vehicle increases, the bias in the position reported by the DSRC also increases.

To follow up on these observations, the vehicle is driven at a different intersection on a westbound lane. An example trajectory from the second intersection showing the UTM Easting and Northing errors is depicted in Figure 3. As displayed in the figure, as the vehicle decelerated and stopped at the red light, the component of the error due to the bias decreased almost to zero. At the beginning of the trajectory, the bias in both UTM Easting and Northing is over 1 meter. The variance in the measurement error is small throughout the trajectory, and gets close to zero as the vehicle slows to a stop. This non-Gaussian behavior in the noise presents a significant challenge for tracking algorithms. Generally, when the bias is a constant amount corrupted by mean-zero Gaussian noise, it can be estimated by including it in the Kalman filter state [1].

We present results later where we compare tracking performance under different amounts of bias by using a simple bias estimation heuristic to "whiten" the measurement noise distribution. One of our main goals is to better understand the robustness of the tracking filters when the mean-zero Gaussian noise assumption is violated.

3.2 Vehicle Kinematics

We examine the performance of state estimation of vehicles at traffic intersections under the constant velocity (CV) and constant acceleration (CA) kinematics models. For a complete description of these models, see [3]. Here, we briefly present them for clarity.

For CV, the vehicle state $\mathbf{x}$ at a discrete time step k is $[x_k, \dot{x}_k, y_k, \dot{y}_k]^\top$, where x_k is UTM Easting, y_k is UTM Northing, $\dot{x_k}$ is speed in the UTM Easting direction, and $\dot{y_k}$ is the speed in the UTM Northing direction. The state can be initialized from measurement o_0 as

$$\begin{bmatrix} x_0 \\ \dot{x}_0 \\ y_0 \\ \dot{y}_0 \end{bmatrix} = \begin{bmatrix} x_0 \\ v_0 \cos\theta_0 \\ y_0 \\ v_0 \sin\theta_0 \end{bmatrix} \tag{2}$$

In the CV model, the velocity is assumed to be constant and acceleration is considered to be a white noise process distributed according to $\mathcal{N}(\mathbf{0}, \mathrm{Q})$, where $\mathbf{0}$ is a four-dimensional vector of zeros. Q is the process noise covariance and is given by:

$$\mathrm{Q} = \sigma_a^2 \begin{bmatrix} \frac{\triangle t^3}{3} & \frac{\triangle t^2}{2} & 0 & 0 \\ \frac{\triangle t^2}{2} & \triangle t & 0 & 0 \\ 0 & 0 & \frac{\triangle t^3}{3} & \frac{\triangle t^2}{2} \\ 0 & 0 & \frac{\triangle t^2}{2} & \triangle t \end{bmatrix} \tag{3}$$

where σ_a is the standard deviation of the acceleration noise process and $\triangle t$ is the difference in seconds between discrete time steps of the tracking filter.

For the CA model, the vehicle state is $[x, \dot{x}, \ddot{x}, y, \dot{y}, \ddot{y}]^\intercal$, where $\ddot{x}$ is the acceleration in the UTM Easting direction and $\ddot{y}$ is the acceleration in the UTM Northing direction. The state can be initialized from o_1 and o_0 at time step $k = 1$ as

$$\begin{bmatrix} x_1 \\ \dot{x}_1 \\ \ddot{x}_1 \\ y_1 \\ \dot{y}_1 \\ \ddot{y}_1 \end{bmatrix} = \begin{bmatrix} x_1 \\ v_1 \cos\theta_1 \\ \frac{v_1 \cos\theta_1 - v_0 \cos\theta_0}{\triangle t} \\ y_1 \\ v_1 \sin\theta_1 \\ \frac{v_1 \sin\theta_1 - v_0 \sin\theta_0}{\triangle t} \end{bmatrix} \tag{4}$$

In the CA model, acceleration is assumed to be constant and the jerk of the vehicle is captured by a white noise process distributed according to $\mathcal{N}(\mathbf{0}, \mathrm{Q})$, where $\mathbf{0}$ is a six-dimensional vector of zeros. The process noise covariance is

$$\mathrm{Q} = q \begin{bmatrix} \frac{\triangle t^5}{20} & \frac{\triangle t^4}{8} & \frac{\triangle t^3}{6} & 0 & 0 & 0 \\ \frac{\triangle t^4}{8} & \frac{\triangle t^3}{3} & \frac{\triangle t^2}{2} & 0 & 0 & 0 \\ \frac{\triangle t^3}{6} & \frac{\triangle t^2}{2} & \triangle t & 0 & 0 & 0 \\ 0 & 0 & 0 & \frac{\triangle t^5}{20} & \frac{\triangle t^4}{8} & \frac{\triangle t^3}{6} \\ 0 & 0 & 0 & \frac{\triangle t^4}{8} & \frac{\triangle t^3}{3} & \frac{\triangle t^2}{2} \\ 0 & 0 & 0 & \frac{\triangle t^3}{6} & \frac{\triangle t^2}{2} & \triangle t \end{bmatrix} \tag{5}$$

where q is a small tunable constant. While the CA model intuitively should be more appropriate for situations where a vehicle decelerates or accelerates at a constant rate, adding more variables to the Kalman filter state tends to degrade the overall performance and stability of the filter in practice.

When the light is green, vehicles generally maintain a constant speed as they approach and drive through the intersection. On the other hand, when the light is red, a vehicle will need to decelerate. One of the goals of this study is to evaluate whether the CV or CA model is superior to the other in these different circumstances. If this turns out to be the case, a multiple model filter could be employed to leverage both kinematics models. In the remainder of this section, we only refer to the CV model when formulating the tracking filters for brevity.

3.3 Modeling the Bias and Variance

In this section, we present the measurement model used to capture the uncertainty in the GPS from the DSRC. We define two covariance matrices, R_1 and R_2, for the LKF and for the EKF and PF respectively. Since the LKF cannot handle nonlinearity in its state and measurement equations, we must define the LKF measurement to be a linear function of the predicted state $\hat{\mathbf{x}}_\mathbf{k}$

$$= \mathrm{H}\hat{\mathbf{x}}_\mathbf{k} + w_1 \tag{6}$$

$$= \begin{bmatrix} 1 & 0 & 0 & 0 \\ 0 & 1 & 0 & 0 \\ 0 & 0 & 1 & 0 \\ 0 & 0 & 0 & 1 \end{bmatrix} \begin{bmatrix} x_k \\ \dot{x}_k \\ y_k \\ \dot{y}_k \end{bmatrix} + w_1 \tag{7}$$

where w_1 is a random variable distributed according to $\mathcal{N}(\mathbf{0}, \mathrm{R}_1)$. We define the covariance as

$$\mathrm{R}_1 = \begin{bmatrix} \sigma_{pos}^2 & 0 & 0 & 0 \\ 0 & \sigma_v^2 & 0 & 0 \\ 0 & 0 & \sigma_{pos}^2 & 0 \\ 0 & 0 & 0 & \sigma_v^2 \end{bmatrix} \tag{8}$$

Given that the raw measurement from the BSM is as shown in Equation 1, we make the necessary nonlinear transformation to put it in a form usable by the LKF but ignore the nonlinearity otherwise.

Since the EKF and PF can model the nonlinearity required to transform the vehicle heading and speed into velocity measurements in the UTM Easting and UTM Northing directions, we define the measurement as a nonlinear function of the predicted state $\hat{\mathbf{x}}_\mathbf{k}$

$$= h(\hat{\mathbf{x}}_\mathbf{k}) + w_2 \tag{9}$$

$$= \begin{bmatrix} x_k \\ y_k \\ \sqrt{\dot{x}_k^2 + \dot{y}_k^2} \\ \arctan 2(\dot{y}_k, \dot{x}_k) \end{bmatrix} + w_2 \tag{10}$$

where w_2 is a $\mathcal{N}(\mathbf{0}, \mathrm{R}_2)$ random variable. The covariance is defined as

$$\mathrm{R}_2 = \begin{bmatrix} \sigma_{pos}^2 & 0 & 0 & 0 \\ 0 & \sigma_{pos}^2 & 0 & 0 \\ 0 & 0 & \sigma_v^2 & 0 \\ 0 & 0 & 0 & \sigma_\theta^2 \end{bmatrix} \tag{11}$$

We need to estimate and remove the biases from w_1 and w_2 so that they actually are approximately mean-zero Gaussian random variables. A simple heuristic for estimating and removing bias is to attempt to center the measurement over the vehicle by using the speed and heading information from the latest measurement. This can be accomplished by positing that the bias increases as the speed increases and decreases to zero as the vehicle slows to a stop. Hence, given a tunable constant α, the speed v_k, and heading θ_k from the latest raw measurement o_k, we can compute a bias vector

$$b(\alpha, v_k, \theta_k) = \begin{bmatrix} \alpha v_k \cos(\theta_k) \\ \alpha v_k \sin(\theta_k) \\ 0 \\ 0 \end{bmatrix} \tag{12}$$

and use it to center w_1 and w_2. The choice of the constant α approximately determines how much correction is needed in order to center the Gaussian distribution of the measurement noise on top of the vehicle as the vehicle speed increases, i.e., make it mean-zero. In Section 4, we show how the tracking performance varies based on the setting of α.

3.4 Tracking Filters

We present the linear and extended Kalman filter equations and briefly describe the particle filter here for the application of tracking vehicles at traffic intersections via DSRC. The reader is directed to [20] and [2] for a more detailed presentation of these algorithms.

We begin by presenting the EKF, show how the LKF can be obtained from a simplification of the EKF, and then finish by describing the PF.

3.4.1 Extended Kalman Filter. Let (μ_k, Σ_k) be the mean and covariance of the multivariate normal distribution representing the vehicle state estimate $\mathbf{x}$ at time k. The predicted mean and covariance $(\hat{\mu}_k, \hat{\Sigma}_k)$ of the vehicle state are computed by the standard Kalman filter predict step equations

$$\hat{\mu}_k = \Phi\mu_k + r_k$$
$$\hat{\Sigma}_k = \Phi\Sigma_k\Phi^\intercal + \mathrm{Q}$$

where r_k is the process noise and is a random variable distributed as $\mathcal{N}(\mathbf{0}, \mathrm{Q})$ and Φ is the appropriate discrete state transition matrix for the CV or CA models (see [3] Section 4.2).

We compute the Jacobian of the nonlinear measurement function h (Equation 9) with respect to $\hat{\mu}_k$. The Jacobian $\nabla h_k = \mathrm{C}_k$ is given by

$$\mathrm{C}_k = \begin{bmatrix} 1 & 0 & 0 & 0 \\ 0 & 0 & 1 & 0 \\ 0 & \frac{\dot{x}_k}{\sqrt{\dot{x}_k^2+\dot{y}_k^2}} & 0 & \frac{\dot{y}_k}{\sqrt{\dot{x}_k^2+\dot{y}_k^2}} \\ 0 & -\frac{\dot{y}_k}{\dot{x}_k^2+\dot{y}_k^2} & 0 & \frac{\dot{x}_k}{\dot{x}_k^2+\dot{y}_k^2} \end{bmatrix} \tag{13}$$

The Jacobian for the CA model is very similar. Using the proper measurement noise w_1 or w_2, we can complete the update step as follows

$$\bar{h}_k = h(\hat{\mu}_k) + w_{1,2} \tag{14}$$
$$\mathrm{K}_k = \hat{\Sigma}_k\mathrm{C}_k(\mathrm{C}_k\hat{\Sigma}_k\mathrm{C}_k^\intercal + \mathrm{R}_{1,2})^{-1} \tag{15}$$
$$\mu_{k+1} = \hat{\mu}_k + \mathrm{K}_k(o_k - \bar{h}_k) \tag{16}$$
$$\Sigma_{k+1} = (I - \mathrm{K}_k\mathrm{C}_k)\hat{\Sigma}_k \tag{17}$$

3.4.2 Linear Kalman Filter. For the implementation of the LKF, the only differences in the above equations are the replacement of h_k with H from Equation 6 and C_k with the identity matrix.

3.4.3 Particle Filter. The PF is a Sequential Monte Carlo technique that uses a set of particles to approximate a probability density. We aim to approximate the posterior $p(\mathbf{x_{k+1}}|o_{k+1})$, which is the result of applying Bayes theorem when we receive a new measurement of the vehicle state o_{k+1}. Our PF implementation is based on the sampling importance resampling (SIR) formulation, as described

Figure 4: The Team Gator Nation NaviGator from the 2007 DARPA Urban Grand Challenge [8] was used for our experiments at the intersections in Gainesville, FL.

in [2]. The algorithm mainly consists of a predict step and an update step followed by a resampling step. For our tracking problem, the state and measurement functions are the same as those used for the EKF formulation.

At a very high level, the particles in the PF can be seen as individual Kalman filters running in parallel, where the estimate of the state is represented as a weighted sum of each Kalman filter. In the update step, we compute the weights for the particles by importance sampling with an importance density q. If the importance density $q(x_{k+1}|x_k, o_k)$ is chosen to be the prior density $p(x_{k+1}|x_k)$, we can simplify the weight update, as it is now given by

$$w_{k+1} \propto w_k p(o_k|x_k). \tag{18}$$

We can easily sample from $p(o_k|x_k)$ as it is just the bias-adjusted measurement likelihood distributed as $\mathcal{N}(\mathbf{0}, \mathrm{R}_2)$. We resample after every step; we find that this is necessary as a large percentage of the weights are assigned probabilities very close to zero. In the next section, we present results from tracking a vehicle as it drives up to an intersection.

4 EXPERIMENTS

4.1 Testbed Details

We collect and time-align DSRC BSMs as well as ground-truth GPS from a vehicle (Figure 4) as it drives towards an intersection in normal traffic. As described in Section 3, data is collected from two intersections; at the first, the vehicle drives on a fairly straight southbound lane, and at the second, the vehicle drives on a gently curving westbound lane. The evaluation dataset contains 6x more data points from the first intersection (Figure 1) than from the second intersection; the runs from the first intersection had larger errors in UTM Northing than from the second intersection, which as a result skewed the data. Essentially, even though our results show larger error in UTM Northing, this does not generalize to all intersections and GPS devices.

For the particle filter, we use 5,000 particles. Due to the large amount of resampling required, this results in extremely slow run times; despite the extra time, the particle filter performs the worst.

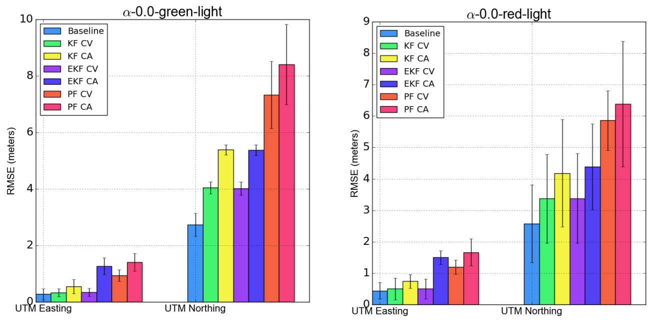

Figure 5: RMSE in UTM Easting and Northing with bias constant $\alpha = 0.0$. With no GPS bias correction, the LKF and EKF show a 48% increase in RMSE compared to the baseline, while the PF showed a 168% increase in RMSE.

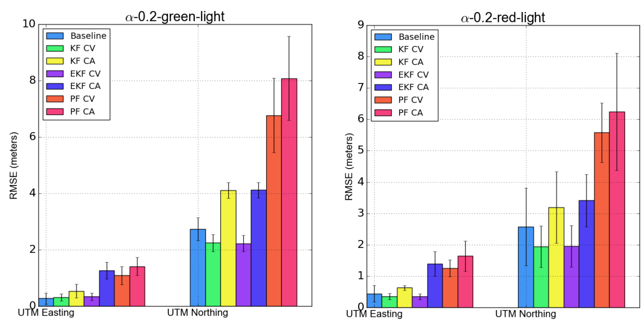

Figure 6: RMSE in UTM Easting and Northing with bias constant $\alpha = 0.2$. With minor GPS bias correction, the LKF and EKF RMSE improves over the baseline by approximately 0.5 meters with the CV model.

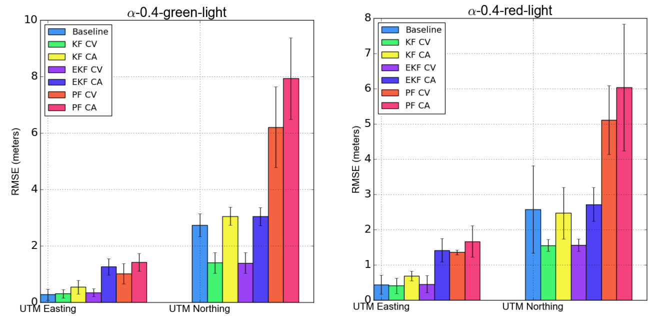

Figure 7: RMSE in UTM Easting and Northing with bias constant $\alpha = 0.4$. The best performance for the tracking filters is seen, with the LKF and EKF RMSE improving over the baseline by 50%. In practice, the clock used by the traffic intersection should already be synchronized within 1 ms [6] of the same UTC reference as the OBUs.

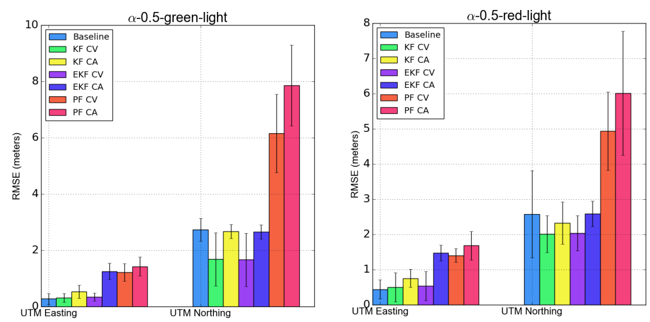

Figure 8: RMSE in UTM Easting and Northing with bias constant $\alpha = 0.5$. The tracking filters showed similar performance to bias constant $\alpha = 0.2$.

For all measurement covariance matrices, we set the standard deviation for position to be 0.5 meters in UTM Easting and Northing. The speed standard deviation is set to 0.1 meters/s and the heading standard deviation is set to 0.1 degrees. For the constant velocity model, the acceleration standard deviation is set to 2 meters/s^2.

4.2 Evaluation Metrics

We aim to identify which state estimation algorithm is the most precise and accurate with respect to the high-precision GPS. For that reason, we compute the root mean square error (RMSE), reproduced in Equation 19, for the entire trajectory of the vehicle from the start of its approach to when it passes through the intersection.

$$RMSE = \sqrt{\frac{\sum_{i=1}^{N}(\mathbf{x_i} - \hat{x}_i)^2}{N}} \tag{19}$$

4.3 Results

As a baseline for comparison, we compute the RMSE between the unfiltered GPS from the DSRC and the ground truth GPS data. We present results of the UTM Easting and Northing RMSE for each state estimation algorithm and each kinematics model. The results are presented as bar graphs with error bars for 1 standard deviation separated by green light and red light runs.

Over all green light runs, the baseline RMSE is 0.276 meters for UTM Easting and 2.73 meters for UTM Northing, with standard deviations of 0.19 meters and 0.4 meters respectively. Similarly, for red light runs, the baseline RMSE is 0.443 meters UTM Easting and 2.57 meters UTM Northing with standard deviations of 0.265 and 1.24 meters.

We ran all state estimation algorithms with bias constants α in the range of [0, 0.5] at increments of 0.05. Figure 5 shows the performance for a bias constant of 0, i.e., no bias estimation is performed. The LKF and EKF have a RMSE that is 48% larger than the baseline, while the PF showed a 168% larger RMSE. This is unsurprising, since these filters add mean-zero Gaussian noise to the biased measurements, which in turn degrades the tracking performance further. For the red light scenarios, the standard deviations are larger and the RMSE is slightly smaller; this is likely due to the fact that the bias in the measurements tends to decrease to zero as the vehicle decelerates. Hence, there is more variability in the tracking RMSE when the light is red. We found that the CA model consistently performs worse than the CV model, as can be seen in Table 1.

The bias constant that produced the lowest RMSE values was $\alpha = 0.4$. The results are shown in Figure 7 with the RMSE values reported in Table 1. For the bias constant of 0.4, the LKF and the EKF performed comparably, improving upon the baseline by almost 50%. The bias constants in the range [0.35, 0.45] produce similar results, with performance degrading slowly beyond this interval.

	Baseline	LKF CV	LKF CA	EKF CV	EKF CA	PF CV	PF CA
green light	0.28, 2.73	**0.31, 1.39**	0.55, 3.05	**0.33, 1.39**	1.26, 3.04	1.1, 6.25	1.42, 7.87
red light	0.44, 2.57	**0.42, 1.55**	0.68, 2.47	**0.45, 1.57**	1.41, 2.72	1.36, 5.18	1.69, 6.10

Table 1: UTM Easting, UTM Northing RMSE in meters for all algorithms with $\alpha = 0.4$. Top two results are in bold. The CA model consistently performs worse than the CV model for situations where the vehicle had to slow to a stop for a red light and maintain speed for a green light.

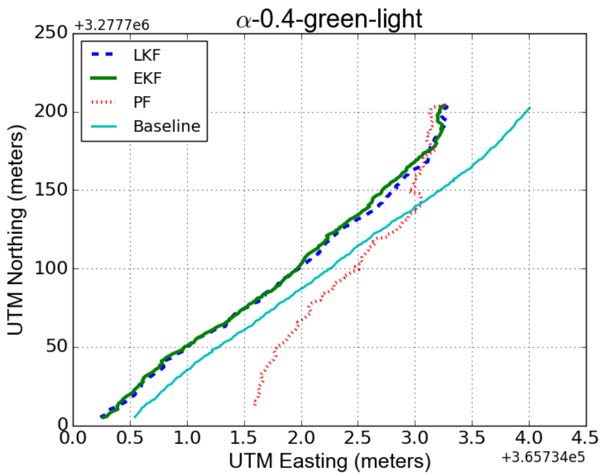

(a)

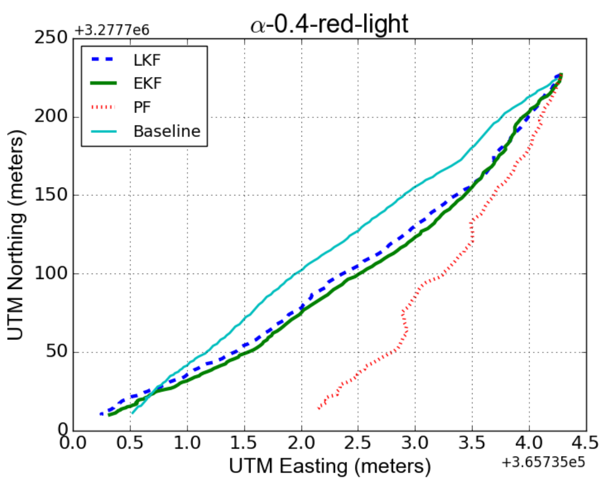

(b)

Figure 9: Demonstration of the tracking algorithms using constant velocity kinematics and a bias constant of 0.4. The global UTM Easting and Northing coordinates of the vehicle are shown as it (a) drives towards a green light at the intersection, maintaining a constant velocity and (b) approaches a red light. The baseline used here is the high-precision GPS. A small bias in the tracking filters in the UTM Northing direction is still noticeable, even after using the simple heuristic to estimate and remove it.

Figures 6 and 8 show the performance for $\alpha = 0.2$ and 0.5; for the LKF and EKF, the RMSE increases by 0.5 meters in UTM Northing for this amount of bias. As stated previously, however, with no bias estimation, the tracking filters actually produce worse estimates of the state due to the violated mean-zero Gaussian assumption.

We believe that the reason why the PF tracked the vehicle so poorly is that the Gaussian distribution we used for the measurement noise is a bad approximation of the actual noise in the DSRC GPS during the intersection approach. In order to better model the uncertainty in the vehicle state, more data could be collected to estimate a non-Gaussian distribution that better captures the noise in the GPS measurements. In a study conducted by [22], it was shown that the multipath effect on GPS in an urban canyon is affected by the speed of the vehicle and the direction of travel with respect to the GPS satellites. Hence, another potential solution is to include information in the BSM about the GPS satellite geometry and estimated clock errors to combine with other details, such as contextual information about the nearby buildings and the current weather, to carry out more sophisticated bias estimation.

In summary, the PF is the least accurate for tracking a connected vehicle with only GPS from BSMs for the current problem formulation. Rather, the constant velocity model paired with the EKF with simple bias estimation is the best option for any intersection geometry; when the heading of the vehicle is not aligned with one of the cardinal directions, the nonlinearity in the transformation applied to the observation extracted from the BSM will become more pronounced. In our dataset, the LKF and EKF performed similarly since the lanes were aligned with the UTM Northing and Easting directions, causing the nonlinear measurement transformation to become approximately linear.

We provide Figures 9a and 9b for a sample green light and red light vehicle trajectory with the estimated vehicle states shown alongside the high-precision GPS data.

5 CONCLUSIONS

In this work, we evaluated the performance of three state estimation algorithms on the task of tracking a DSRC-equipped vehicle at a traffic intersection. The linear Kalman filter, extended Kalman filter, and particle filter with constant velocity and constant acceleration models were compared by examining the RMSE of their state estimates with respect to a high-precision GPS sensor. In summary:

- Without GPS bias estimation, the tracking filters actually produce worse state estimates than the unfiltered GPS
- The linear Kalman filter and the extended Kalman filter both perform equally well on our dataset, achieving a significantly lower RMSE than the particle filter and a lower RMSE than the unfiltered GPS by almost 50% after removing some of the measurement bias with a simple heuristic
- The constant velocity model outperforms the constant acceleration model for both green light and red light scenarios
- The GPS measurement bias observed in our dataset is time-varying and the noise distribution appears to be non-Gaussian.

This bias can be due to time synchronization errors, systematic errors introduced when applying coordinate transformations, and environmental effects that can add noise to the GPS signal such as multipath. A Gaussian approximation to the noise distribution is shown to be unsuitable for modeling the uncertainty in the GPS from BSMs

The results from this research are preliminary, and will be extended by incorporating more data and other traffic sensors such as radar, LiDAR, and video cameras via data fusion to produce better state estimates. The time-varying bias with non-Gaussian noise distribution in GPS from OBUs in urban environments poses many challenges for tracking vehicles based on data from DSRC. We will conduct more tests at other urban intersections and under different weather conditions to further characterize this measurement uncertainty.

ACKNOWLEDGMENTS

The authors would like to thank Dr. Carl Crane, Patrick Neal, Mahmoud Pourmehrab, Aschkan Omidvar, and Marilo Martin-Gasulla from the AVIAN team as well as Emmanuel Posadas and Joe Crackel from the City of Gainesville Public Works Department for assistance with conducting field tests.

This work is supported by the National Science Foundation under grant 1446813 and the Florida DOT under grant BDV31, TWO 977-45. Any opinions, findings, and conclusions or recommendations expressed in this material are those of the author(s) and do not necessarily reflect the views of the National Science Foundation.

REFERENCES

[1] William S Agee and Robert H Turner. 1972. *Optimal Estimation of Measurement Bias.* Technical Report. National Range Operations Directorate White Sands Missile Range NM Analysis and Computation Div.

[2] M Sanjeev Arulampalam, Simon Maskell, Neil Gordon, and Tim Clapp. 2002. A tutorial on particle filters for online nonlinear/non-Gaussian Bayesian tracking. *IEEE Transactions on signal processing* 50, 2 (2002), 174–188.

[3] Samuel Blackman and Robert Popoli. 1999. Design and analysis of modern tracking systems. *Norwood, MA: Artech House, 1999.* (1999).

[4] Qi Chen, Tobias Roth, Ting Yuan, Jakob Breu, Florian Kuhnt, Marius Zöllner, Miro Bogdanovic, Christian Weiss, Jörg Hillenbrand, and Axel Gern. 2015. DSRC and radar object matching for cooperative driver assistance systems. In *Intelligent Vehicles Symposium (IV), 2015 IEEE.* IEEE, 1348–1354.

[5] DSRC Committee et al. 2009. *Dedicated short range communications (DSRC) message set dictionary.* Technical Report. Soc. Automotive Eng., Warrendale, PA, USA, Tech. Rep. J2735.

[6] DSRC Committee et al. 2016. *On-Board System Requirements for V2V Safety Communications.* Technical Report. Soc. Automotive Eng., Warrendale, PA, USA, Tech. Rep. J2945.

[7] CAMP Vehicle Safety Communications Consortium et al. 2005. Vehicle safety communications project: Task 3 final report: identify intelligent vehicle safety applications enabled by DSRC. *National Highway Traffic Safety Administration, US Department of Transportation, Washington DC* (2005).

[8] Carl D Crane III, David G Armstrong II, Antonio A Arroyo, Antoin Baker, Doug Dankel, Greg Garcia, Nicholas Johnson, Jaesang Lee, Shannon C Ridgeway, Eric M Schwartz, et al. 2007. Team gator nation's autonomous vehicle development for the 2007 DARPA Urban challenge. *JACIC* 4, 12 (2007), 1058–1085.

[9] Soufiene Djahel, Nafaa Jabeur, Robert Barrett, and John Murphy. 2015. Toward V2I communication technology-based solution for reducing road traffic congestion in smart cities. In *Networks, computers and communications (ISNCC), 2015 international symposium on.* IEEE, 1–6.

[10] Nour-Eddin El Faouzi and Lawrence A Klein. 2016. Data Fusion for ITS: Techniques and Research Needs. *Transportation Research Procedia* 15 (2016), 495–512.

[11] John Esposito. 2017. *An Application of DSRC Between Connected Vehicles and Intelligent Transportation Systems.* Master's thesis. University of Florida.

[12] Rui Meireles, Mate Boban, Peter Steenkiste, Ozan Tonguz, and Joao Barros. 2010. Experimental study on the impact of vehicular obstructions in VANETs. In *Vehicular Networking Conference (VNC), 2010 IEEE.* IEEE, 338–345.

[13] Pinar Oguz-Ekim, Khaled Ali, Zahra Madadi, Francois Quitin, and Wee Peng Tay. 2016. Proof of concept study using DSRC, IMU and map fusion for vehicle localization in GNSS-denied environments. In *Intelligent Transportation Systems (ITSC), 2016 IEEE 19th International Conference on.* IEEE, 841–846.

[14] M. Pourmehrab, L. Elefteriadou, S. Ranka, and M. Martin-Gasulla. 2017. Optimizing Signalized Intersections Performance under Conventional and Automated Vehicles Traffic. *ArXiv e-prints* (July 2017). arXiv:1707.01748

[15] Swapna Raghunath, P Visalakshmi, and Karam Sridhar. 2013. GPS datum conversion and kalman filtering for reducing positional errors. *Asian Journal of Computer Science & Information Technology* 1, 5 (2013).

[16] Ahmed Hamdi Sakr and Gaurav Bansal. 2016. Cooperative localization via DSRC and multi-sensor multi-target track association. In *Intelligent Transportation Systems (ITSC), 2016 IEEE 19th International Conference on.* IEEE, 66–71.

[17] N Salameh, G Challita, S Mousset, A Bensrhair, and S Ramaswamy. 2013. Collaborative positioning and embedded multi-sensors fusion cooperation in advanced driver assistance system. *Transportation Research Part C: Emerging Technologies* 29 (2013), 197–213.

[18] Guni Sharon and Peter Stone. 2017. A Protocol for Mixed Autonomous and Human-Operated Vehicles at Intersections. In *Agent-Based Modeling of Urban Systems, The 2nd International Workshop on.*

[19] Macheng Shen, Ding Zhao, and Jing Sun. 2016. Enhancement of low-cost gnss localization in connected vehicle networks using rao-blackwellized particle filters. In *Intelligent Transportation Systems (ITSC), 2016 IEEE 19th International Conference on.* IEEE, 834–840.

[20] Sebastian Thrun, Wolfram Burgard, and Dieter Fox. 2005. *Probabilistic robotics.* MIT press.

[21] Lei Wang, Paul D Groves, and Marek K Ziebart. 2013. GNSS shadow matching: Improving urban positioning accuracy using a 3D city model with optimized visibility scoring scheme. *Navigation* 60, 3 (2013), 195–207.

[22] Peng Xie and Mark G Petovello. 2015. Measuring GNSS multipath distributions in urban canyon environments. *IEEE Transactions on Instrumentation and Measurement* 64, 2 (2015), 366–377.

[23] Kaidi Yang, S Ilgin Guler, and Monica Menendez. 2016. Isolated intersection control for various levels of vehicle technology: Conventional, connected, and automated vehicles. *Transportation Research Part C: Emerging Technologies* 72 (2016), 109–129.